

李志坚文集

(下)



科学出版社

www.sciencep.com

李志坚文集

(下)

科学出版社

北京

图书在版编目(CIP)数据

李志坚文集. 下/李志坚著. —北京: 科学出版社, 2010

ISBN 978-7-03-027090-0

I. 李… II. 李… III. 电子技术-文集 IV: TN-53

中国版本图书馆 CIP 数据核字(2010)第 051105 号

责任编辑: 刘红梅 杨 凯 / 责任制作: 董立颖 魏 谨

责任印制: 赵德静

北京东方科苑图文有限公司 制作

<http://www.okbook.com.cn>

科 学 出 版 社 出版

北京东黄城根北街 16 号

邮政编码: 100717

<http://www.sciencep.com>

北京天利彩色印刷有限公司 印刷

科学出版社发行 各地新华书店经销

*

2010 年 5 月第 一 版 开本: B5(720×1000)

2010 年 5 月第一次印刷 印张: 110 3/4 插页: 8

印数: 1—1 100 字数: 1 736 000

定 价: 360.00 元

(如有印装质量问题, 我社负责调换)

目 录

战略展望

✦ A Discussion on the Extension of Moore's Law 关于摩尔定律延伸的探讨	1025
✦ 微电子技术发展与物理学	1033
✦ GMR 生物传感器研究进展	1046
✦ 从 ULSI 芯片的性能能量效率展望 21 世纪信息电子学的发展	1053

器件物理

✦ XPS Characterization on the Mn-Doped BST Thin Films Prepared by Sol-Gel Method 溶胶凝胶法制备的 Mn 掺杂 BST 薄膜的 XPS 特性	1077
✦ Fabrication of (100) Orientated PZT Thin Films for MEMS Applications 用于 MEMS 的(100)取向 PZT 薄膜的制备	1084
✦ Characteristics of Silicon-Based $Ba_xSr_{1-x}TiO_3$ Thin Films Prepared by a Sol-Gel Method 溶胶凝胶法制备的硅基 BST 薄膜的特性	1091
✦ Preparation and Etching of Silicon-Based Piezoelectric Thin Films for Integrated Devices 用于集成器件的硅基压电薄膜的制备和刻蚀	1098
✦ Modeling and Simulation of Thin-Film Bulk Acoustic Resonators 薄膜体声波谐振器的建模和仿真	1105
✦ $Ba_{0.5}Sr_{0.5}TiO_3$ Ferroelectric Thick Films with Uniform Thickness and Its Applications to RF MEMS Devices 厚度均匀的 BST 铁电厚膜及其在射频 MEMS 器件中的应用	1112
✦ Measurement of Thermal Conductivity of Buried Oxides of Silicon-on-Insulator Wafers Fabricated by Separation by Implantation of Oxygen Technology 氧注入制作的 SOI 中埋氧热导率的测量	1121
✦ Mn 掺杂 BST 薄膜的制备与表征	1126

▶ Characterization of Mn-Doped $Ba_{1-x}Sr_xTiO_3$ Thin Films Prepared by the Sol-Gel Method 溶胶凝胶法制备的 Mn 掺杂 BST 薄膜的特性	1132
▶ Investigation of Thermal Property of Novel DSOI MOSFETs Fabricated with Local SIMOX Technique 局部注氧隔离制作的新型 DSOI MOSFET 的热学特性研究	1137
▶ Preparation and Properties of PLZT Thick Films on Silicon 硅基 PLZT 厚膜的制备和特性研究	1143
▶ DSOI, SOI 和体硅 MOSFET 的特性测量比较	1150
▶ PZT Based MFS Structure for FeFET 用于 FeFET 的 PZT 基 MFS 结构	1157
▶ Fabrication of High Quality PZT Thick Film Using Lift-Off Technique 剥离法制作高品质 PZT 厚膜	1164
▶ Fabrication and Properties of Silicon-Based PLZT Thin Films for MFSFET Applications 用于 MFSFET 的硅基 PLZT 薄膜的制备和特性	1171
▶ Optical and Structural Investigation of Stacked Ge Quantum Dots 多层 Ge 量子点的光学特性和结构研究	1178

集成电路技术

▶ 一种多分辨率组合的模糊神经网络分类器	1185
▶ 模拟神经元电路实现研究现状与进展	1197
▶ 一种基于超盒表示的规则提取方法	1215
▶ Fuzzy Petri Nets for Rule-Based Pattern Classification 用于规则模式分类的模糊 Petri 网	1225
▶ Using Learning Samples to Construct Fuzzy Logic Systems with the Application to Inverted Pendulum Control 使用学习样本构建的模糊控制系统在倒立摆中的应用	1234
▶ Fabrication and Properties of Silicon-Based PZT Thin Films for MFSFET Applications 用于 MFSFET 的硅基 PZT 薄膜的制备和特性	1239
▶ Design of an Analog Adaptive Fuzzy Logic Controller 一种模拟自适应模糊控制器的设计	1246
▶ 基于电荷泵实现的模糊控制器去模糊电路设计	1256
▶ 新结构重心法去模糊单元电路设计	1262

系统集成技术

- ▶ 高灵敏度微机械薄膜的设计、模拟与优化 1271
- ▶ Design Optimization of Beam-Like Ferroelectrics-Silicon
Microphone and Microspeaker
梁式铁电-硅微麦克风和扬声器的设计优化 1281
- ▶ Study of Anisotropic Etching of (100) Si with Ultrasonic Agitation
超声波激励的(100)硅各向异性腐蚀研究 1288
- ▶ Single-Chip Condenser Miniature Microphone with a High Sensitive
Circular Corrugated Diaphragm
具有高灵敏度圆形纹膜的单芯片电容式微麦克风 1297
- ▶ 硼预淀积对自组织生长 Ge 量子点尺寸分布的影响 1305
- ▶ Preparation and Characterization of a Sol-Gel Prepared
Ferroelectric Sandwich Structure
溶胶凝胶法铁电三明治结构的制备和表征 1312
- ▶ 硅基衬底 $Ba_{0.5}Sr_{0.5}TiO_3$ 厚膜制备的 sol-gel 新方法 1319
- ▶ Comparative Studies of Novel Capacitive Transducers with
Non-Planar Diaphragms
新型非平面振膜电容式换能器的比较研究 1326
- ▶ High Quality Ferroelectric Capacitor for FeRAM Applications
用于 FeRAM 的高品质铁电电容 1335
- ▶ A Novel Single-FET Cell and Array Architecture for Ferroelectric
Nonvolatile Memories
一种新型的单 FET 铁电非挥发存储器的单元和阵列结构 1341
- ▶ A Novel Miniature Optical Switch Array with Cantilever
Micromirrors Driven by PZT Films
具有 PZT 薄膜驱动悬臂式微镜的新型微光学开关阵列 1346
- ▶ 硅微机械悬浮结构电感的设计与制作工艺研究 1353
- ▶ On the Single-Chip Condenser Miniature Microphone Using DRIE
and Backside Etching Techniques
使用 DRIE 和背面刻蚀技术的单芯片电容式微麦克风 1361
- ▶ Surface Micromachining of Bulk Acoustic Wave Filters
体声波滤波器的表面微加工 1373
- ▶ Optimization of PZT-Based Radio-Frequency Filters
PZT 基射频滤波器的优化 1380
- ▶ A Novel Ferroelectric Based Microphone
一种新型的铁电微麦克风 1387

▼ 大束流 Co 离子注入形成 CoSi_2/Si Schottky 结的特性	1392
▼ Piezoelectric and Ferroelectric Films for Microelectronic Applications 微电子应用中的压电和铁电薄膜	1398
▼ High-Frequency Properties of PZT for RF-Communication Applications 用于射频通讯的 PZT 的高频特性	1407
▼ Miniature Microphone with Silicon-Based Ferroelectric Thin Films 基于硅基铁电薄膜的微麦克风	1413
▼ Design of a Triaxial Piezoelectric Accelerometer 三轴压电加速度计的设计	1419
▼ Experimental Results on Drain and Source on Insulator MOSFETs Fabricated by Local SIMOX Technology 局部注氧隔离制作的 DSOI MOSFET 的实验结果	1426
▼ 用于射频领域的高调节范围 MEMS 压控电容	1435
▼ Fabrication of High-Quality PZT-Based Piezoelectric Microphone 基于高品质 PZT 的压电微麦克风的制作	1441
▼ High Quality PZT Thick Films Using Silicon Mold Technique for MEMS Applications 用于 MEMS 硅模技术制备的高品质 PZT 厚膜	1448
▼ $\text{Ni}_{81}\text{Fe}_{19}$ 层厚度对自旋阀巨磁电阻性能的影响	1454
▼ 用于集成磁传感器的热稳定巨磁电阻自旋阀 ¹⁾	1457
▼ 用于衬底隔离的选择性氧化多孔硅厚膜的制备	1461
▼ 热环境对微机械多晶硅薄膜电阻电特性的影响	1464
▼ Fabrication Planar Coil on Oxide Membrane Hollowed with Porous Silicon as Sacrificial Layer 多孔硅作为牺牲层的镂空氧化物薄膜上平面线圈的制作	1472
▼ Self-Assembled SiGe Islands with Uniform Shape and Size by Controlling Si Concentration in Islands 通过控制 Si 的浓度实现具有均匀形状和大小的自组装 SiGe 岛	1481
▼ 高介电常数介质 RF MEMS 开关的制作研究	1486
▼ The Key Technologies in Silicon Based Microwave and RF MEMS Device Fabrication 硅基微波和射频 MEMS 器件制作中的关键技术	1492
▼ The Study on a Voltage Controlled Capacitor with Complex Membrane 具有复合薄膜的压控电容研究	1501
▼ Design of Coils Inductively-Tuned RF MEMS Shunt Switches Using Novel Modeling Method 利用新型建模方法进行线圈电感调谐的 RF MEMS 旁路开关设计	1509

▶ Reactive Ion Etching and Ion Beam Etching for Ferroelectric Memories 用于铁电存储器的反应离子刻蚀和离子束刻蚀	1517
▶ Key Integration Techniques and Issues for Silicon-Based Ferroelectric Devices 硅基铁电器件中的关键集成技术和问题	1523
▶ Study of a Ferroelectrics-Silicon Integrated Microspeaker and Microspeaker Array 铁电-硅集成微麦克风和扬声器研究	1533
▶ 三板板型 RFMEMS 压控电容的分析与制作	1542
▶ RIE 对巨磁电阻自旋阀磁性能的影响	1545
▶ 氧化多孔硅上制作 Cu 电感的研究	1551
▶ 两侧下拉电极 MEMS 压控电容的分析和优化	1557
▶ 高阻硅上 RF-MEMS 共面波导设计及测量研究	1569
▶ 一种 K 波段双桥电容式 RF MEMS 开关的设计与制作	1578
▶ 斜拉梁结构的 RF-MEMS 开关制作研究	1587
▶ 一种 X 波段 RF MEMS 开关的设计与制作研究	1593
▶ Dependence of GMR on NiFe Layer Thickness in High Sensitive Simple Spin Valve 高灵敏度简单自旋阀中 GMR 和 NiFe 层厚度的关系	1600
▶ 介质表面形貌对射频微机械开关隔离度的影响	1607
▶ Study on Large-Inductance Inductors Using Double-Layer Coils on HR Substrate 高阻衬底上双层线圈大值电感研究	1614
▶ Study on the Reliability of Capacitive Shunt RF MEMS Switch 旁路电容式 RF MEMS 开关的可靠性研究	1622
▶ Bonding Packaging of a SP4T RF MEMS Switch SP4T RF MEMS 开关的键合封装	1630
▶ A Passive Low-Pass Filter on Low-Loss Substrate 低损耗衬底上的一种无源低通滤波器	1638
▶ Micro Acoustic Devices Using Piezoelectric Films 基于压电薄膜的微声学器件	1647
▶ Uniformity Improvement of PZT Based Ultrasonic Transducer PZT 基超声换能器性能一致性的改进	1657
▶ A Dielectric-Bridge-Type MEMS Series Contact Switch for 0~10GHz Applications 应用于 0~10GHz 的介质桥膜型 MEMS 串联接触开关	1665

▶ Study on Dynamic Characterization of a Shunt Capacitive RF MEMS Switch 一种旁路电容式 RF MEMS 开关的动态特性研究	1672
▶ Thermal Conductivity Measurements of Ultra-Thin Single Crystal Silicon Films Using Improved Structure 应用改进结构的超薄单晶硅薄膜热导率的测量	1678
▶ Fabrication of Si_xN_y Nanomechanical Structures Using Traditional Lithography and Gas Isotropic Etching 使用传统光刻和气体各向同性刻蚀的氮化硅纳米机械结构的制作	1685
▶ 多层复合结构应变硅材料的生长和特性	1692
▶ 一种新型三谐振点电容式 RF MEMS 开关	1700
▶ Directivity Optimization of PZT Based Microspeaker Array PZT 基微麦克风阵列的方向性优化	1706
▶ Effect of Annealing Temperature on Properties of Sputtered PZT Thin Films 退火温度对溅射法制备的 PZT 薄膜性能的影响	1715
▶ Realization of a Series Contact MEMS Switch with SiON Dielectric Bridge 一种 SiON 介质桥膜结构的串联接触 MEMS 开关的实现	1723

战略展望

A Discussion on the Extension of Moore's Law¹⁾

Abstract Both theory and ITRS predict that the scaling of conventional silicon CMOS is going to approach its ultimate. Several emerging devices based on different new mechanism are proposed as possible successors. But still, as classical 2-level switches, they have common limits of quantum uncertainty and thermodynamic fluctuation. In order to further enhance and improve the ability and performance of ULSI systems, either more efficient devices or processing systems with new model and architecture are required. In this article, these topics are briefly discussed in unified view of the product of device delay time and its power dissipation.

I . Introduction

Almost three decades ago Gordon Moore of Intel Corporation observed that the number of transistors per chip had been doubling annually for years^[1]. This astute observation has become known as “Moore's Law”. Today the Moore's Law is still valid. But this trend certainly has its ultimate. When decreasing the channel length and supply voltage, some secondary effects will become more and more significant, and the increasing leakage current I_{leak} will increase the stand-by power dissipation. When this increasing stand-by power dissipation exceeds some percents (10% for example) of maximum power dissipation and the transconductance is no longer larger than the output conductance, our scaling down strategy meets its ultimate.

This article will have a review and discussion on the extension of Moore's Law from the energy point of view of switching transition. In section II a discussion of ultimate CMOS, base on theory, ITRS and experiments, is given. In section III data

1) In: International Conference on Solid-State and Integrated Circuits Technology Proceedings, ICSICT, v1, 2004 7th International Conference on Solid-State and Integrated Circuits Technology Proceedings, ICSICT 2004, 2004:251–254 (Coauthor: Tiefu Li).

of some recently developed emerging devices are involved. In section IV the limit of classical 2-level switching devices will be shown. Finally in section V, a discussion on how to overcome the Heisenberg limit is given.

II. Ultimate Si CMOS

Si CMOS is the foundation of today's IC technology. The enhancement of IC performance is mainly by appropriately scaling down of device dimension and voltage. But this scaling is not boundless^[2]. When scaling down the channel length and voltage, some secondary effects, such as SCE, DIBL, Punch-Through and Hot-Carrier Effects, will tend to be more and more significant, which make the leakage current I_{leak} and stand-by power dissipation increasing. When the stand-by power dissipation in total power dissipation reaches a definite proportion (different for different applications) and device output conductance gets over the transconductance. MOSFET's scaling down meets its ultimate^[3]. For example, ITRS has set that the maximum power dissipation (P_{max}) of unit chip area is 100W, and for HP(High Performance) CMOS devices the stand-by power dissipation, P_{st} , should be less than 10% of P_{max} . With this stand-by power dissipation and supply voltage (V_{dd}), we can get the maximum leakage current (I_{leak}). And then the effective channel length, L_{eff} , thickness of oxide layer, t_{ox} , and finally the ultimate E_{b} and performance can be decided. For Si CMOS there are also limits on signal delay, which is mainly because of the finite velocity of electrons. With the saturated velocity of electrons (v_{sat}) we can deduce the minimum delay, $\tau_{\text{min}} = L/v_{\text{sat}}$, and the maximum delay with the minimum supply voltage, $\tau_{\text{max}} = L^2/\mu V$. Thus for every possible E_{b} , CMOS can be designed on a segment of $\log\tau$ - $\log P$ plot with τ_{min} and τ_{max} as terminals.

For every 2-level switch we have $E_{\text{b}} = P\tau$ and plot $\log\tau$ vs $\log P$ gives a straight line with constant E_{b} . For CMOS $E_{\text{b}} = \frac{1}{2}CV^2$ where C and V are capacitance and applied voltage of the switch. Fig. 1 shows the scaling down trend of Si CMOS on this plot, data is from ITRS(2003). The points represent the delay, and power dissipation of Si CMOS devices with different channel length and corresponding V_{dd} and V_{T} . Two lines at the left lower corner represent the limits set by Heisenberg Uncertainty Principle and Thermodynamics^[4]. First of all, from this plot we can see that with devices scaling down, points move towards the lower left corner of the plot, that is the smaller delay and power dissipation, better performance. Second, as mentioned before, the scaling down strategy has its ultimate. The theoretical predicted value for ultimate CMOS E_{b} is approximately the same as that proposed by ITRS^[5]. For HP devices, using given P_{max} and P_{st} , it has been found that ultimate

$L_g \approx 10\text{nm}$, corresponding ultimate $E_b \approx 10^{-18}\text{ J}$ for 300K. So the corresponding constant E_b line in the $\log P$ - $\log \tau$ plot is the ultimate E_b of Si CMOS for HP use. Third, for one E_b , the devices also have limit on signal delay time as mentioned before. The delay time can only be between the τ_{\min} and τ_{\max} . As approximately shown in the plot, the area surrounded by three lines is the zone for Si CMOS. All Si CMOS devices can not be out of this region.

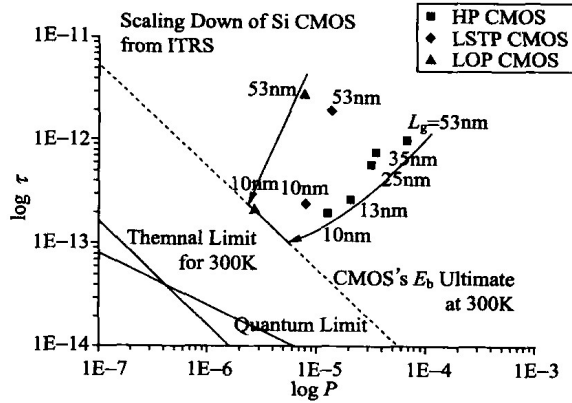


Fig. 1 Scaling down trend of Si CMOS from ITRS

Recently many research centers and companies, such as IME of CAS^[6], Stanford, IBM and Intel, have developed MOSFET with nano-scale channel length (from 6nm to 70nm). Fig. 2 shows their properties (data from [6] and IEDM (2001 ~ 2003)) comparing with the trend from ITRS. We can see from this plot clearly that these experimental points are all in the discussed region of Si CMOS, especially they are all above the CMOS's E_b limit. They can have different power dissipation or delay, but no one of them is located beyond the limit of Si CMOS devices.

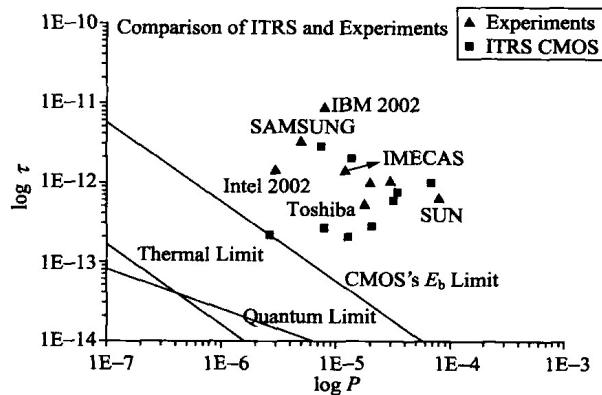


Fig. 2 Scaling down trend from experiments and ITRS

III. Emerging Devices

In order to overcome the Si CMOS limit recently a series devices based on new mechanism are proposed. Some perspective examples are discussed in this section.

1. CNT

CNT(Carbon Nano Tube), as a kind of natural nanowires, has been shown to have larger mobility than that of bulk silicon and due to one dimensional transportation the ballistic transport is expected in it. Further, since CNT has a very large breakdown electric field (up to 10^6 V/cm), the carrier drift velocity can greatly exceed that in silicon inversion layer.

We can see from Fig. 3 and Fig. 4 (data extracted from ITRS(2003)) that by scaling Si CMOS, the electron mobility decreases, while the electron drift velocity nearly keeps constant. So we can not reduce delay as we want. This is velocity saturation. But it is not this case for CNT. By ballistic transport in CNT, nearly constant mobility with increasing of electric field and thus velocity over-shoot can be expected.

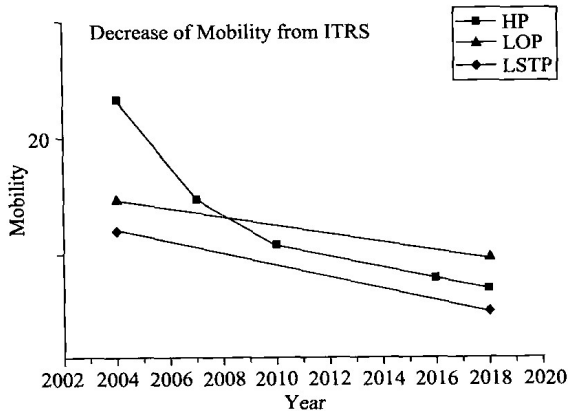


Fig. 3 The change of mobility of CMOS

We have three sets of data about CNT shown in Fig. 5. The EXP is an experimental data from IEDM, $L_g = 260\text{nm}$, $V_{dd} = 2.5\text{V}$. Set I and II are deduced from EXP, with $L_g = 25\text{nm}$, $V_{dd} = 2.5\text{V}$ and $L_g = 25\text{nm}$, $V_{dd} = 0.5\text{V}$, respectively, with assumption of ballistic transport. We can see from Fig. 5 that a CNT of 260nm long has nearly the same delay as a CMOS transistor of 25nm long but a larger power dissipation. When we reduce CNT's length and keep voltage invariant as in case I, it has a very small delay that CMOS can not reach but still a larger power dissipation. But when we reduce both the voltage and length, CNT has not only small delay but

also small power dissipation. We should notice in case II the CNT has already had a E_b smaller than that of ultimate CMOS. And moreover in case II CNT also overcomes the delay time barrier of CMOS.

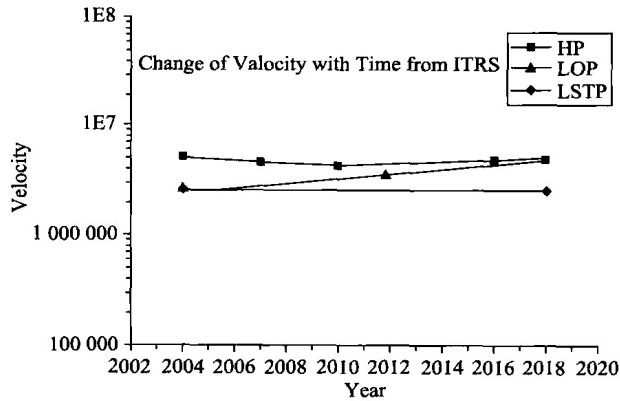


Fig. 4 The change of velocity of CMOS

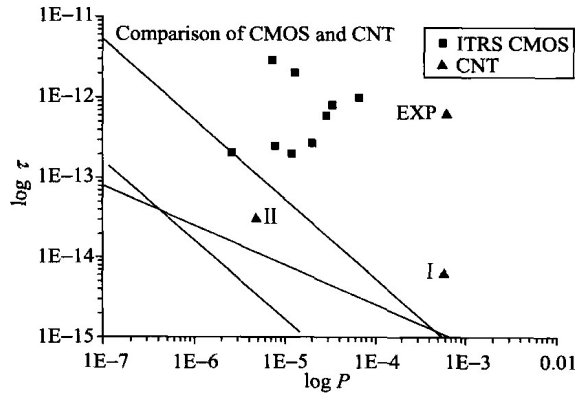


Fig. 5 Comparison of ITRS CMOS and CNT

2. Other Emerging Devices

Other emerging devices (generally called nano-devices) include RSFQ (Rapid Single Flux Quantum), Optical Switch, NEMS (NanoElectroMechanical Systems) Switch, Molecular Switch, etc. We won't discuss them in detail, they are still in stage of laboratory investigation. In Fig. 6 the corresponding data presented in ITRS (2003) for these devices are quoted, indicated and compared with Si CMOS and CNT.

As can be seen in the plot there is a much wider span of those kinds of devices. At this moment we ignore the two points. Bio and Quan, which will be discussed in section V. We can see NEMS has the smallest power dissipation and largest delay, while Optic devices have the smallest delay but quite a large power dissipation. The others, Molecule Switch and RSFQ all have their own characters. Some of these data

exceed the Si CMOS limit thus able to improve the IC technology.

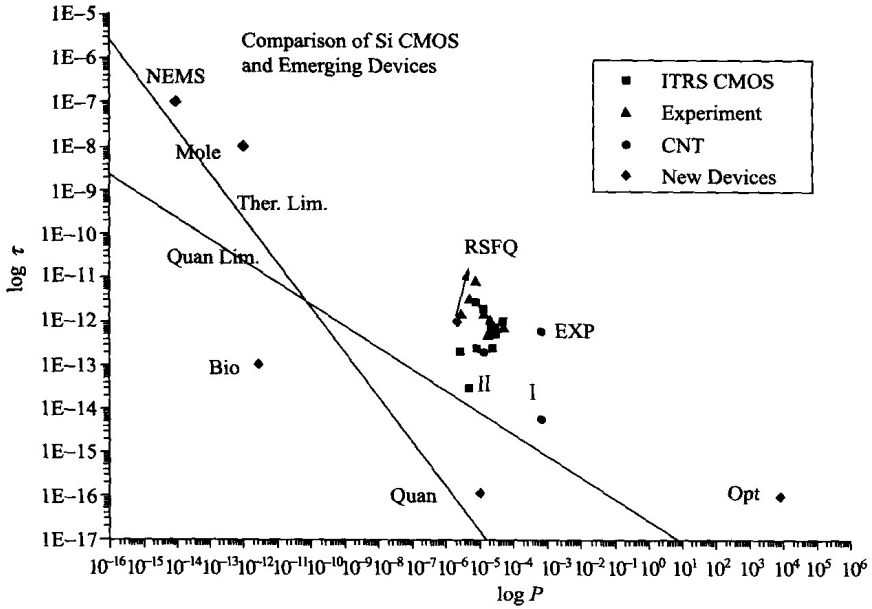


Fig. 6 Comparison of CMOS and emerging devices

IV. Limits of Classical 2-level Switching Devices

As shown in Fig. 6, although many emerging nanodevices can have performance (either speed-power product or speed and power separately) better than that of ultimate CMOS, they are still limited by two common lines corresponding to two fundamental physical principles of thermodynamics and quantum mechanics. Due to thermal noise the energy separation of two binary signal digits should be $E_b \geq \gamma k T$ ($\gamma = \ln 2$), as discussed by Shannon, where k is Boltzmann constant and T is absolute temperature. On the other hand by quantum uncertainty principle $E_b \tau \geq \hbar$, that is $P \tau^2 \geq \hbar$. Thus these two straight lines on the $\log \tau$ vs $\log P$ plot are the lowest boundary for all devices based on classical 2-level switching. We can see from Fig. 6 that any 2-level switching devices, including classical Si CMOS and emerging devices, does not exceed these limits.

Fig. 7 shows an ideal 2-level switching device. We assume when the particle on the left of the potential, it represents state "0" and when on the right it is state "1". The particle's passing through of the potential represents a switching transition from "0" to "1" or "1" to "0". We propose that the device is working in the critical region of quantum limit, so that $\Delta x \Delta p = \hbar$ and $\tau \Delta E = \hbar$, i. e. $\Delta x = \hbar / \sqrt{2m^* E_b}$ and $\tau = \hbar / E_b$. It indicates that by choosing appropriated parameter Δx (that is a in Fig. 7)